Materials Today Bio 26 (2024) 101084

Contents lists available at ScienceDirect

Materials Today Bio

journal homepage: www.journals.elsevier.com/materials-today-bio

Real time monitoring peripheral nerve function with ICG and BDA-ICG by NIR-II fluorescence imaging

Xiaoqi Yang [a,b,1], Yuanyi Wang [c,1], Chunrong Qu [b], Boyu Tan [b], Minjin Wang [d], Senrui Li [a], Jinsheng Huang [a], Jiangnan Li [a], Mengyuan Fang [e,*], Zhen Cheng [b,**], Nan Zhou [a,***]

[a] Department of Orthopedics, The First Affiliated Hospital of Zhengzhou University, No. 1 Jianshe East Road, Zhengzhou, 450052, Henan, China
[b] State Key Laboratory of Drug Research, Molecular Imaging Center, Shanghai Institute of Materia Medica Chinese Academy of Sciences, Chinese Academy of Sciences, Shanghai, 201203, China
[c] Department of Spinal Surgery, The First Hospital of Jilin University, Orthopedics Center, Jilin University, Changchun, 130021, China
[d] Department of Laboratory Medicine, West China Hospital of Sichuan University, Chengdu 610041, China
[e] Department of Ophthalmology, The First Affiliated Hospital of Zhengzhou University, Zhengzhou University, Zhengzhou, 450052, China

A B S T R A C T

Neuroanatomical tract tracers are important for studying axoplasmic transport and the complex interconnections of the nervous system. Though traditional fluorescent tracers are widely used, they have several prominent drawbacks when imaging, including low resolutions and low tissue penetrations and inability to be supervised dynamically within a long peripheral nerve during the long term. Here, we explored the potential of ICG as a neural tracer for axoplasmic transport and for the first time demonstrated that ICG could be used to detect transport function within peripheral nerve by near-infrared region II (NIR-II) imaging. On basis of this finding, a novel bi-directional neural tracer biotinylated dextran amine-indocyanine green (BDA-ICG) was prepared and characterized with better long-term stability and higher nerve-to-background ratio than ICG in vivo, and successfully imaged the injured peripheral nerve from the healthy one within 24 h. Our results show that BDA-ICG are promising neural tracers and clinically available dyes with NIR-II emission tail characteristics as ICG.

1. Introduction

Peripheral nerve injury (PNI) is one of the most common neurological disorders in daily life, affecting over one million patients worldwide each year [1,2]. Although peripheral nerves possess a unique ability to regenerate after injury, the loss of this capacity over time frequently results in a poor functional recovery. The slow rate of axonal regeneration negatively affects reinnervation of distal target organs, leading to disappointing functional outcomes and high rates of disability. Current diagnosis of PNI relies mainly on clinical symptoms caused by peripheral nervous system (PNS) dysfunction, which is often at an advanced stage by the time they appear. Besides, clinical methods, including muscle strength testing, electromyography and intraoperative electrophysiological examination, are commonly used for detecting the axonal regeneration and evaluating the functional recovery of peripheral nerve [3,4]. However, the lack of timeliness, objectivity, accuracy and visualization is believed to be the major limitation of these methods. Therefore, an early, straightforward and reliable assessing method is crucial for diagnosis of PNI and tracking the nerve regeneration, thus better predicting the outcomes.

Fluorescence imaging is the simplest and most flexible method of detection. Its advantages include no ionizing radiation, fast signal feedback, strong multi-signal collection, and high sensitivity. Owing to these distinct benefits, fluorescence imaging has found extensive applications in the diagnosis of diseases, evaluation of drug distribution and metabolism, and image-guided precision surgery [5,6]. There have been many fluorescent tracers used in neuroanatomical tracing to study the complex interconnections of the nervous system, including fluorescent dyes (carbocyanine, rhodamine, fast blue) and fluorescent compounds (dextran molecules, biotinylated dextran amines) [7]. In our previous studies, carbonized polymer dots and Au nanodots were conjugated with Cholera toxin B (CTB) or biotinylated dextran amine (BDA, an anterograde neural tracer which produces sensitive and detailed labelling) to make novel fluorescent neural tracers with significant advantages, such as excellent optical properties, physiochemical stability, and biocompatibility [8–10]. Unfortunately, the excitation and emission

* Corresponding author.
** Corresponding author.
*** Corresponding author.
E-mail addresses: fccfangmy@zzu.edu.cn (M. Fang), zcheng@simm.ac.cn (Z. Cheng), fcczhoun@zzu.edu.cn (N. Zhou).
[1] These authors contributed equally: Xiaoqi Yang, Yuanyi Wang.

https://doi.org/10.1016/j.mtbio.2024.101084
Received 27 January 2024; Received in revised form 18 April 2024; Accepted 3 May 2024
Available online 6 May 2024

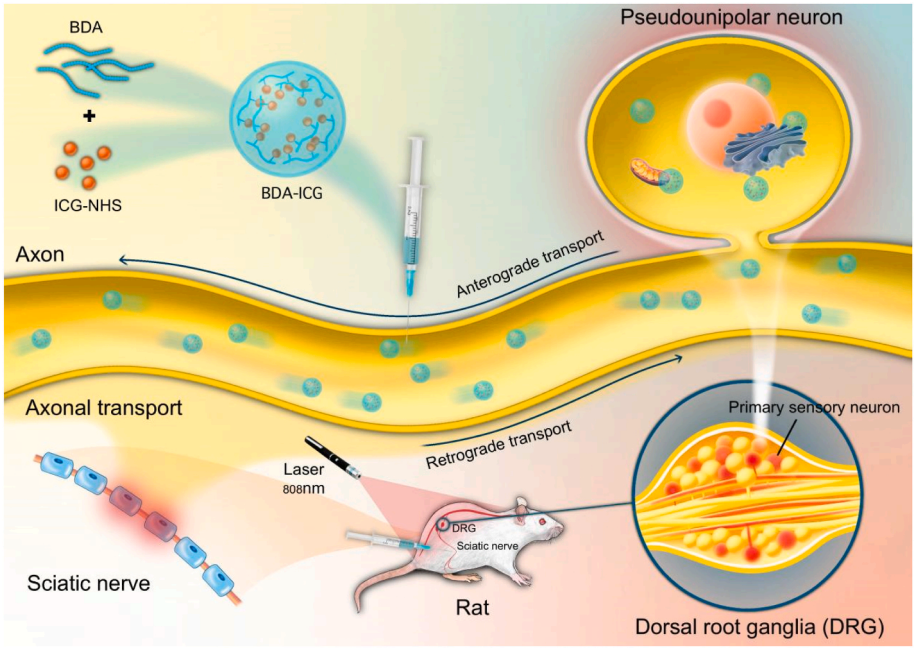

Scheme 1. Illustration of the experimental process.

wavelengths of these tracers are primarily located in the visible (400–700 nm) or near infrared I (NIR-I, 700–950 nm) bands, in which the resolution and tissue penetration of fluorescence imaging are low due to strong autofluorescence, scattering effects and significant absorption by biological tissues, thus do not reflect physiological and pathological information accurately [11]. NIR-II, which is mostly detected between 1000 and 1700 nm, however, shows reduced photon scattering, less tissue autofluorescence and less light-tissue interaction. These excellent characteristics greatly improve the sensitivity, resolution and depth of fluorescence imaging [12]. Without a doubt, over the past ten years, biomedical imaging in NIR-II has emerged as a hotspot for research. However, there are limited data on the in vivo NIR-II monitoring the function of the peripheral nerve with neural tracers.

ICG is the only FDA-approved cyanine dye in the U.S [13]. It has been used in medical applications since the mid-1950s and is a relatively toxic fluorescent iodide dye with rapid liver clearance. ICG has shown good in vivo NIR-II imaging outcomes in small animals. Its emission wavelength is around 800 nm, and its tailband emission can extend into the NIR-II [14]. Though ICG has been frequently utilized in ocular angiography, tumor surgery, and medical diagnostics of liver function, the research on imaging with ICG in peripheral nerves is extremely sparse [15]. In fact, whether ICG could directly label the peripheral nerve is controversial. Some studies believe ICG is a non-specific fluorescent contrast agent without nerve-targeting properties [16]. However, recently some reports found that preoperative intravenous injection of ICG was able to visualize the neuroanatomical structures such as the thoracic sympathetic ganglion and the genitourinary nerve in patients during the surgery and the immunofluorescence results showed ICG mainly located in axons [17,18]. Based on these interesting findings, we speculated that ICG might be neurophilic and have the potential to be used as a neural tracer for NIR-II imaging.

Dextran is a non-toxic and hydrophilic polysaccharide that can be used as a neural tracer when conjugated with various fluorescent dyes or biotinylated to form an affixed neural tracer [19]. In 1992, Veenman first reported the favorable properties of BDA as a new anterograde tracer that produced sensitive and detailed labeling [20]. Then, subsequent studies confirmed that BDA 10 000 MW is effective for anterograde tracing in many species and has the advantages of long shelf life, high sensitivity, and easy to be combined with a wide range of fluorescent tracers and various immunohistochemical techniques [21,22]. All these studies suggest that BDA is a promising ligand for the synthesis of novel neural tracers.

In the present work (Scheme 1), we first explored the potential of ICG as a peripheral neural tracer and used ICG for the first time in vivo in NIR-II window to visualize axoplasmic transport. Then, we developed a novel neural tracer biotinylated dextran amine-indocyanine green (BDA-ICG), which has a better long-term stability in vivo and a higher signal-to-noise ratio compared to ICG, offering the possibility of diagnosis and tracking during the long recovering period. Also, we demonstrated the transport mechanism of BDA-ICG and ICG within the nerve was microtubule. Last, we successfully used BDA-ICG for early diagnosis of injured peripheral nerves and long-term tracking of nerve regeneration.

2. Materials and methods

2.1. Materials

ICG were purchased from Aladdin Scientific; ICG-NHS and *N,N*-Diisopropylethylamine (DIPEA, 99 %) were purchased from J&K Scientific; BDA (D1956) were purchased from Molecular Probes; Colchicine was purchased from GlpBio; Anti S100β, anti NF200, anti β-Tubulin Polyclonal antibody were purchased from Proteintech; Dimethyl sulfoxide (DMSO, 99.9 %) and *N,N*-Dimethylformamide (DMF, 97 %) were purchased form LeYan; DMEM were purchased from Thermo Fisher; DAPI, Lyso-Tracker Green (C1047S) and Mito-Tracker Green (C1048) were purchased from Beyotime; ER-Tracker Green (BODIPY® FL Glibenclamide) was purchased from YEASEN Biotech; PC12 cells were purchased from the Chinese Academy of Sciences. The cells were cultivated in a DMEM medium in a humidified incubator with 5 % CO^2 at 37 °C. All reagents were used as received without further purification. Deionized water was used in all experiments (18.2 MΩ cm^{-1}). The 33-gauge 5 μL microsyringe was purchased from Hamilton.

2.2. Preparation of BDA-ICG complex

Conjugation of ICG to biotinylated dextran amine (BDA, 10 000 MW) was performed in the following procedures. Commercially available

BDA (10 000 MW) was supplied in lyophilized form. BDA (4 mg) and ICG-NHS (0.9 mg) were dissolved in DMF (0.5 mL) solution, and DIPEA (5 μL) was added. After for overnight stirring at room temperature, the reaction was quenched with diH^2O (8 mL) followed by dialyzed (7000 Da) 2 days, then freeze-dried to obtain green powder.

2.3. Characterization of BDA-ICG

2.3.1. Spectral characterization of the BDA-ICG

The absorption spectra of BDA-ICG and ICG were measured by ultraviolet–visible-2600 spectrometer (SHIMADZU) with the background correction for solvents such as deionized water and DMSO. The NIR-II fluorescence emission spectrum was captured by an 755 nm laser-excited spectrometer (MARS-IRIS, Artemis Intelligent Imaging, Shanghai, China).

2.3.2. Photostability of BDA-ICG

ICG was used as a reference fluorophore. ICG and BDA-ICG were dissolved in PBS and irradiated with an 808 nm laser for 30 min. Photostability was determined by measuring the region of interest (ROI) and comparing the fluorescence intensity with the initial fluorescence signal.

2.3.3. TEM imaging and DLS

A solution of BDA-ICG in PBS at a concentration of 100 μg/mL was prepared by ultrasonic treatment for 15 min and filtration. The aqueous solutions were dropped onto the carbon-coated grid (200 mesh) and dried. The TEM imaging pictures were detected by 120 kV transmission electron microscope. The nanoparticle size of BDA-ICG was further verified by dynamic light scattering (DLS).

2.3.4. Standard UV–Vis absorption curve

The apparent absorbance has been demonstrated to be proportional to the ICG concentration by Beer-Lambert Law [23]. First, we prepared different concentrations of ICG as standard samples and measured the UV–visible absorption spectra of this batch of ICG samples to obtain the corresponding data, including wavelength, concentration and absorbance. Next, we recorded the values of absorbance (Abs) at the peak wavelength for different concentrations of ICG standard samples, and corresponded these recorded Abs values to their ICG concentrations respectively. Then, taking the Abs value as parameter x and the concentration of ICG as parameter y, at least 5 concentrations were selected, and the standard curve formula of y(concentration) = k*x(Abs) + b was calculated [24] (Essentially, it's a variant of Beer-Lambert law, A = εlc). In this way, a linear quantitative relationship between absorbance and concentration of ICG was obtained. Under the same experimental conditions, the estimated concentration of ICG in samples could be easily and quickly calculated by determining the Abs value at the same wavelength. By this method, we obtained the concentration of ICG contained in a certain concentration of BDA-ICG sample, and thus roughly got the mass percentage of ICG in BDA-ICG.

2.4. Animals

All experimental animals were purchased from the Shanghai Experimental Animal Center (Shanghai). All animal procedures were performed under the guidelines approved by the Institutional Animal Care and Use Committee (IACUC) of the Shanghai Institute, Chinese Academy of Sciences. Six-weeks-old female nude mice and 200–220g Sprague Dawley (SD) rats (n = 3 per group) were obtained for imaging studies and placed in the Shanghai Institute of Materia medical under our approved animal protocols.

2.5. Cell culture and imaging

2.5.1. Cell culture

Undifferentiated rat adrenal pheochromocytoma cells (PC12 cells) were cultured in DMEM containing high glucose (Gibco), all of which were supplemented with 10 % FBS and 1 % penicillin-streptomycin. Nerve growth factor (NGF, 25 ng/mL) was added, and the cells were cultured for 3 days to produce the neuronal phenotype. The cells were expanded in tissue culture dishes and kept in a humidified atmosphere of 5 % CO2 at 37 °C. The medium was changed every other day. A confluent monolayer was detached with 0.5 % trypsin and dissociated into a single-cell suspension for inoculation.

2.5.2. Cell imaging

For microscopy, PC12 cells were plated in 35 mm glass-bottom at a cell density of 1×10^4 cells per dish. After the cells attached to the substrates, they were treated with 25 ng/mL NGF for 3 days before conducting experiments. NGF-treated PC12 cells were incubated with BDA-ICG (100 μg/mL, FBS) and ICG (10 μg/mL, FBS) for 30 min. After 3 times washing, Lyso-Tracker Green, Mito-Tracker Green, and ER-Tracker Green were added to determine the intracellular distribution of BDA-ICG. The process was performed in accordance with the manufacturer's instructions. We used a confocal microscope (STELLARIS 8, Leica, German) with a 63 × oil immersion objective lens to observe.

2.5.3. Quantitative colocalization analysis

The quantitative colocalization analysis of BDA-ICG or ICG in different organelles were performed in two different methods as previously described [25,26]. For the first method, we performed linear quantitative fluorescence analysis of representative individual cells. Briefly, the quantitative data were obtained by measuring the fluorescence intensity of different position in a linear distance of 30 μm through the *Fiji* software. BDA-ICG and ICG were showed as red channel and the commercial organelle dyes were showed as green channel. Then, we normalized the fluorescence intensity of the two channels and placed them in the same graph. By analyzing the trend of fluorescence intensity at the same position, we could easily determine whether BDA-ICG and ICG enter the different organelles. For the second method, we analyzed all the cells showed in the merge image. In brief, we performed the colocalization analysis of images of BDR-ICG and ICG with images of commercial organelle dyes by *Fiji* software. Then, the software output the scatterplot and generated the Pearson Correlation Coefficient and the Manders Overlap Coefficient.

2.6. In vivo imaging of BDA-ICG and ICG after intravenous administration

Six-week-old female BALB/c nude mice (n = 3 per group) were chose and anesthetized by isoflurane inhalation and fixed in the prone or supine position, and BDA-ICG (100 μL, 1 μg/μL) was injected intravenously. All the NIR-II fluorescence images at different time points were performed on an in vivo imaging system (MARS, Artemis Intelligent Imaging, Shanghai, China).

2.7. Anterograde or retrograde tracing with BDA-ICG and ICG in the peripheral nervous system

2.7.1. Surgical procedures

SD rats were randomized for the experimental group and surgical procedures were performed under isoflurane anesthesia (3 % induction and 2 % maintenance) with the rats placed properly in the prone position. The left sciatic nerve was exposed just below the sciatic notch under sterile conditions and then injected with BDA-ICG (5 μL, 1 μg/μL) or ICG (5 μL, 0.1 μg/μL). To reduce the negative effect on the sciatic nerve, we used a 5 μL Hamilton microsyringe to gently insert the epineurium, followed by slowly injecting BDA-ICG or ICG into one position at an approximate rate of 1 μL/1 min, retaining the needle in the nerve for 5–10 min and withdrawing the needle after confirming no leakage. The whole process of injection should consume at least 20 min. The incision was closed and sterilized.

2.7.2. NIR-II imaging for the transport of the BDA-ICG and ICG

Anterograde and retrograde tracing imaging was performed using MARS-Pathfinder in vivo stereomicroscope imaging system (Artemis Intelligent Imaging, Shanghai, China).

Anterograde tracing within 24 h: During the imaging process, rats were performed under isoflurane anesthesia (3 % induction and 2 % maintenance) with a proper prone position. All the NIR-II fluorescence images at different time points were performed on an in vivo NIR-II imaging system with the sciatic nerve exposed. After the observation, the incision was closed and sterilized, and the rats were allowed to recover on heated pads before being returned to their home cage.

Long-term anterograde tracing for 2 w: During the imaging process, rats were performed under isoflurane anesthesia (3 % induction and 2 % maintenance) with a proper prone position. An NIR-II fluorescence imaging system was used to observe the migration of the injected BDA-ICG and ICG with images taken in a time course (0 d and 14 d post-injection) with the sciatic nerve exposed. After the observation, the incision was closed and sterilized, then the rats were allowed to recover on heated pads before being returned to their home cage.

Retrograde tracing at 24 h post-injection: At 24 h post-injection, the rats were euthanized. The bilateral L4 and L5 DRGs and the lumbar spinal cord were dissected out carefully and then imaged using the NIR-II fluorescence imaging system.

2.8. Imaging of colchicine pre-treated model

2.8.1. Pre-treat with colchicine

The surgical procedures were performed under isoflurane anesthesia (3 % induction and 2 % maintenance) with the SD rats placed properly in the prone position. Both the left and right sciatic nerves were exposed just below the sciatic notch under sterile conditions and then injected with 5 μL colchicine (5 μg/μL) respectively [27]. After the injection, the incision was closed and sterilized, then the rats were allowed to recover on heated pads before being returned to their home cage.

2.8.2. Injected with BDA-ICG and ICG

36 h after pre-treated with colchicine, both the left and right sciatic nerves were exposed under sterile conditions and then injected with BDA-ICG (5 μL, 1 μg/μL) or ICG (5 μL, 0.1 μg/μL), under isoflurane anesthesia (3 % induction and 2 % maintenance) with the rats placed properly in the prone position. After the injection, the incision was closed and sterilized, then the rats were allowed to recover on heated pads before being returned to their home cage.

2.8.3. In vivo imaging of colchicine pre-treated model

Anterograde and retrograde tracing imaging was performed using MARS-Pathfinder in vivo stereomicroscope imaging system (Artemis Intelligent Imaging, Shanghai, China).

Anterograde tracing at 24 h post-injection: At 24 h post-injection, the rats were euthanized. Both the left and right sciatic nerves were exposed and imaged using the NIR-II fluorescence imaging system.

Retrograde tracing at 24 h post-injection: At 24 h post-injection, the rats were euthanized. The bilateral L4 and L5 DRGs and the lumbar spinal cord were dissected out carefully and then imaged using the NIR-II fluorescence imaging system.

2.9. Imaging of crush injury model

2.9.1. Surgical operations

SD rats were randomized for the experimental group and surgical procedures were performed under isoflurane anesthesia (3 % induction and 2 % maintenance) with the rats placed properly in the prone position. The left sciatic nerve was exposed just below the sciatic notch under sterile conditions and then crushed using Dumont #5/45 forceps for 15 s twice and an internal of 10 s. After the nerve injury, the left sciatic nerve was injected with BDA-ICG (5 μL, 1 μg/μL) at the proximal to the crush site. To reduce the negative effect on the sciatic nerve, we used a 5 μL Hamilton microsyringe to gently insert the epineurium, followed by slowly injecting BDA-ICG into one position at an approximate rate of 1 μL/1 min, retaining the needle in the nerve for 10 min and withdrawing the needle after confirming no leakage. The whole process of injection should consume at least 20 min. After the injection, the incision was closed and sterilized, then the rats were allowed to recover on heated pads before being returned to their home cage.

2.9.2. In vivo imaging of BDA-ICG in crush injury model

Long-term anterograde tracing for 7 d: During the imaging process, rats were performed under isoflurane anesthesia (3 % induction and 2 % maintenance) with a proper prone position. An NIR-II fluorescence imaging system was used to observe the migration of the injected BDA-ICG with images taken in a time course (0 d, 1 d, 4 d and 7 d post-injection) with the sciatic nerve exposed. After the observation, the incision was closed and sterilized, and the rats were allowed to recover on heated pads before being returned to their home cage.

2.10. Preparation of tissue sections and fluorescence imaging

Anterograde tracing: After injecting the BDA-ICG solution or ICG solution for 24h, 48 h and 14 d, the rats were euthanized and intravenously injected with 0.9 % saline and 4 % paraformaldehyde through the left ventricle. Sciatic nerve tissue including the distal to the injection site was harvested. Fresh tissues were immediately embedded using optimal cutting temperature compound (OCT), rapidly frozen in liquid nitrogen, and transported on dry ice for frozen sectioning. Sciatic nerve longitudinal sections (10–12 μm thickness) were obtained using a frozen section machine. The prepared tissue slices were observed under a fluorescence microscope at magnifications of 4 × and 25 × . The whole process was conducted in the dark.

Retrograde tracing: After injecting the BDA-ICG solution or ICG solution for 24 h, the rats were euthanized and intravenously injected with 0.9 % saline and 4 % paraformaldehyde through the left ventricle. The lumbar spine and back of rats were carefully incised, and bilateral L5 DRGs were removed. Fresh tissues were immediately embedded using OCT, rapidly frozen in liquid nitrogen, and transported on dry ice for frozen sectioning. L5 DRG longitudinal sections (12–15 μm thickness) were obtained using a frozen section machine. The prepared tissue slices were observed under a fluorescence microscope at magnifications of 10 × . The whole process was conducted in the dark.

2.11. Immunofluorescence staining

Sciatic nerve was harvested at 24 h and 48 h post-injection and the longitudinal sections and transverse sections of the nerve tissue were prepared as above described. The sections were dried by a dryer for 30 min first and fixed with 4 % paraformaldehyde (PFA) for 10 min. Then the sections were closed with the blocking solution (Beyotime) at room temperature for 1 h, and then incubated with the primary antibody at 4 °C overnight, followed by incubation with the secondary antibody at room temperature in the dark for 1 h. Finally, the cells were counterstained with DAPI, and the photomicrographs were taken using a fluorescence microscope. Schwann cells were labeled with anti S100β, nerve fibers were labeled with anti-NF200, nuclei were stained with DAPI, microtubules were labeled with anti β-Tubulin Polyclonal antibody.

2.12. Statistical analysis

Data were expressed as means ± standard error of the mean. Differences between groups were assessed using unpaired two-tailed t tests. p *values* < 0.05 was considered statistically significant. GraphPad Prism 8.0.

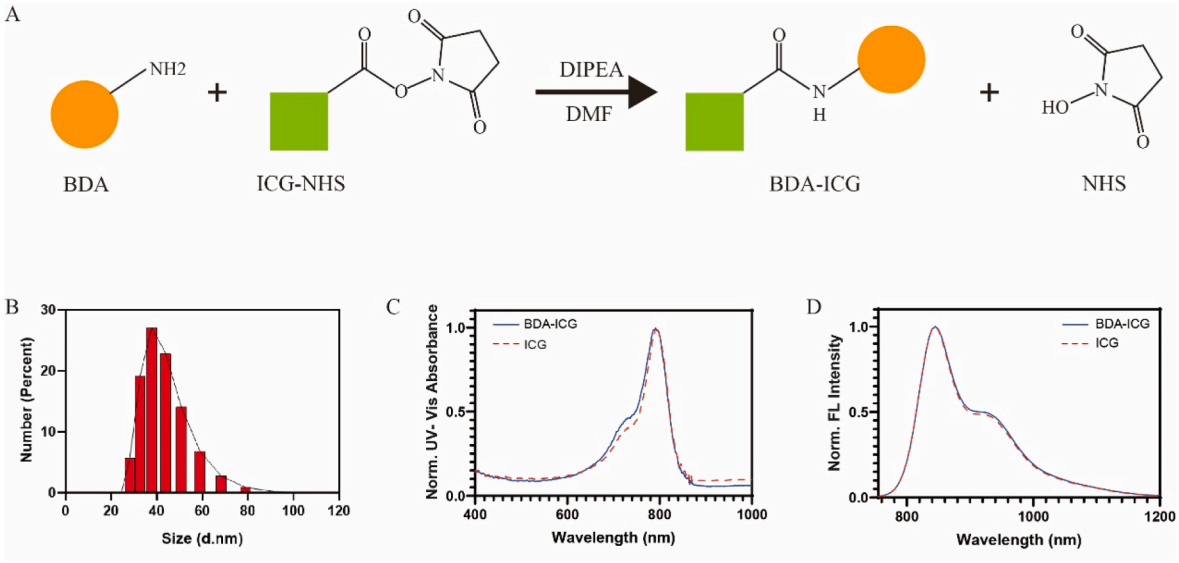

Fig. 1. Preparation and characterization of BDA-ICG. (A) Schematic illustration of the synthesis of BDA-ICG. (B) Size distribution histogram of BDA-ICG based on DLS. (C) UV–Vis absorption spectra of BDA-ICG and ICG. (D) Emission (Ex = 755 nm) spectra of BDA-ICG and ICG.

3. Results and discussion

3.1. Preparation and characterization of BDA-ICG conjugates

The basic features and properties of ICG are not mentioned too much in this paper, as there have been many related studies and reports on it [28]. As shown in Fig. 1 A, BDA was conjugated with ICG-NHS by esterification reaction to produce BDA-ICG. TEM and DLS were used to study the size and shape of BDA-ICG. TEM image suggested (Fig.S1 A) that BDA-ICG behaved as nanoparticles and tend to form aggregates. The data of DLS showed that the diameter of BDA-ICG lay between 20 and 100 nm (Fig. 1 B), which was basically consistent with that of the TEM image. For the UV–Vis absorption spectra, BDA-ICG exhibited an absorption peak at around 780–800 nm, and the curve was similar to that of ICG (Fig. 1C). The emission spectra was shown from 755 nm to 1200 nm, and the peak was around 835 nm. (Fig. 1 D). The spectrum of BDA-ICG were similar to ICG, indicating that the optical properties of ICG changed little after the conjugation. We tested the photostability of BDA-ICG and ICG by continuous laser irradiation for 30 min (Fig.S1 B). The fluorescence intensity of both BDA-ICG and ICG sharply decreased after laser irradiation for only 5 min, which demonstrated that BDA-ICG and ICG had the same fluorescence quenching. With the help of the fluorescence absorption standard curves of ICG and BDA-ICG (Fig.S1 C and D; Fig. S2), the estimated mass ratio of ICG to BDA in the BDA-ICG (ICG: BDA, 1 : 9) was obtained. This ratio provided us with data support for the subsequent determination of reagent concentration.

BDA-ICG not only had its maximum absorption closer to the laser 808 nm excitation wavelength, but also has trailing fluorescence emission in the NIR-II. All these characterization data confirmed that BDA and ICG were successfully coupled together, and that the newly synthesized BDA-ICG retained the fluorescence property of ICG. BDA-ICG had promising potential for NIR-II fluorescence imaging.

3.2. In vivo imaging and safety assessment of BDA-ICG after intravenous administration

After analyzing the optical properties of BDA-ICG, we investigated its distribution and metabolic properties in vivo after intravenous injection. As shown in Fig. 2 A, at the initial stage after tail vein injection of BDA-ICG (100 μL, 1 μg/μL) into nude mice, the fluorescent signal was mostly concentrated in the liver, kidney and intestine. Then, the fluorescent signals of most organs gradually decayed or even disappeared with the progress of time and metabolism. At 24 h post-injection, only the liver retained obvious fluorescent signals (Fig. 2 A). We obtained the major internal organs of experimental animals, including heart, liver, spleen, lung, kidney and intestines, at different time points (4 h, 8 h and 24 h post-injection) to analyze the distribution of the BDA-ICG in these isolated organs. The results showed that after intravenous injection, BDA-ICG was largely concentrated in the liver, intestine and kidney at 4 h and 8 h, while only the liver showed a high signal at 24 h, which was consistent with the results observed by in vivo imaging (Fig. 2 B). To further investigate whether intravenous administration of BDA-ICG would cause acute damage to the major metabolic organs, the major organs of the experimental animals were harvested at 24 h post-injection for H&E analysis, and no obvious pathological abnormality was observed compared with that of the healthy nude mice (Fig. 2C).

ICG is mainly metabolized by the liver, however, the in vivo and in vitro imaging results of BDA-ICG showed that its main metabolic organs were the liver, kidneys, and intestine, indicating that BDA-ICG has a different metabolic pathway from ICG. The difference may be caused by BDA as our pervious study showed the similar bio-distribution with BDA-CDs [9]. There was basically no fluorescence of BDA-ICG being observed in the kidney and intestine but liver at 24 h post-injection, suggesting that BDA-ICG could be removed from the body from different metabolic routes when being administrated intravenously, which may partially alleviate the metabolic burden of the liver. Furthermore, there was no notable acute liver structural damage from H&E analysis, though there was still strong in vivo fluorescent signal in it. These results seem to provide a preliminary indication that BDA-ICG has good metabolism and biosafety by intravenous distribution.

3.3. In vitro distribution of BDA–ICG

To further understand the cell biological behavior of BDA-ICG, the in vitro biodistribution of BDA-ICG should be elucidated distinctly. We chose the PC12 cell line, which is commonly used in the field of neurobiology, for intracellular imaging studies. We evaluated the intracellular trafficking and localization of BDA-ICG (Fig. 3. A, C and E) and ICG (Fig. 3. B, D and F) by co-staining with various commercially organelle-specific fluorescent probes, including Lyso-Tracker Green, Mito-Tracker Green, and ER-Tracker Green. Then, we quantitatively analyzed the colocalization of BDA-ICG (Fig. S4A, C and E) or ICG (Fig. S4B, D and F) with different organelles. Confocal images showed that both BDA-ICG and ICG were able to be taken up by PC12 cells, and

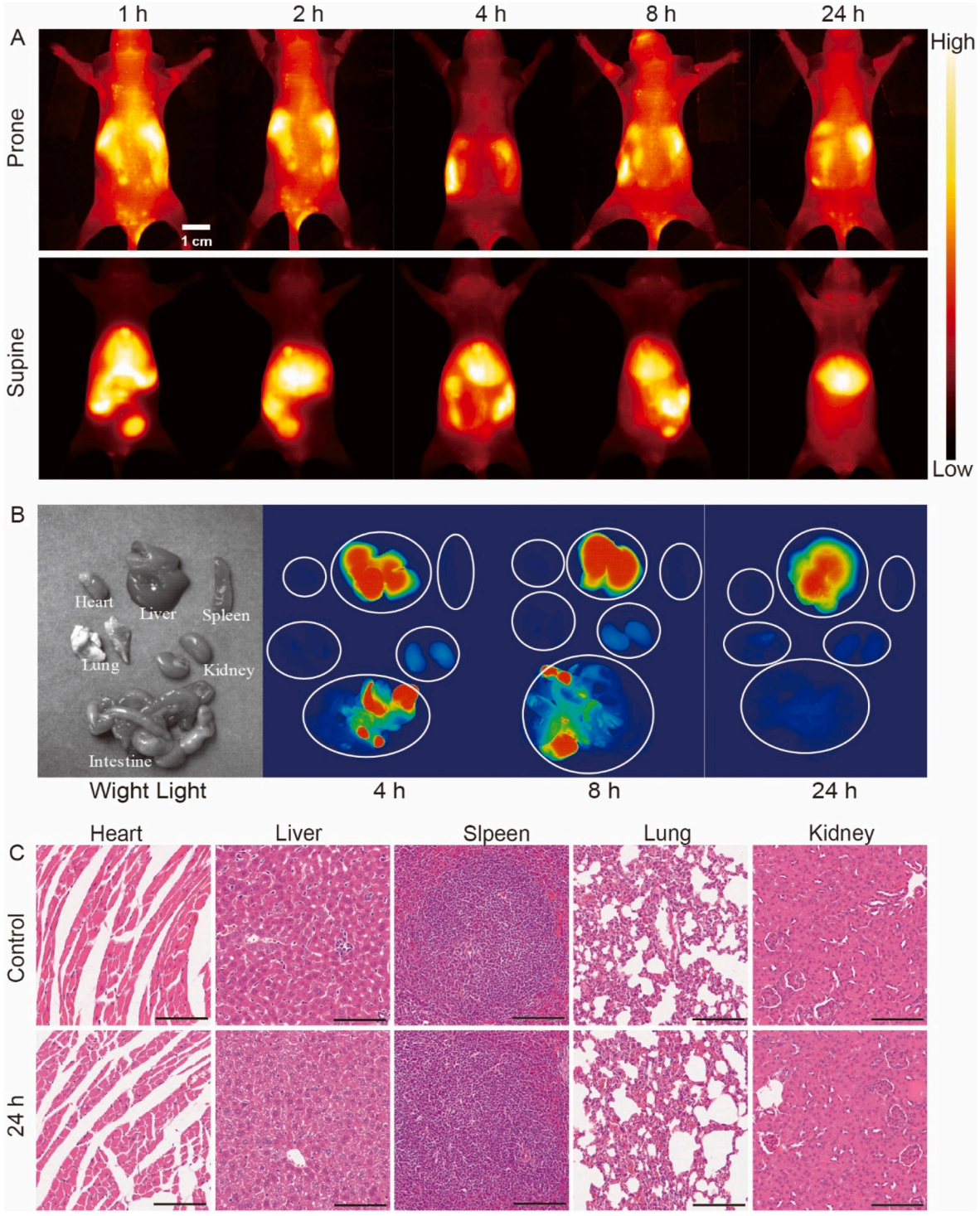

Fig. 2. Biodistribution and biosafety of BDA-ICG. (A) Time-dependent NIR-II fluorescence imaging of mice intravenously injected with BDA-ICG (Excitation wavelength: 808 nm; Filter: 1000 LP; Exposure time: 80 ms; Laser Power: 38.6 mW cm^{-2}). (B) Bright field photographs and NIR-II fluorescence images of the major organs harvested at 4 h, 8 h, and 24 h post-injection (Excitation wavelength: 808 nm; Filter: 1000 LP; Exposure time: 80 ms; Laser Power: 38.6 mW cm^{-2}). (C) Representative H&E staining of major organs collected from the mice in control and BDA-ICG group at 24 h post-injection. The scale bar is 100 μm.

both them were diffusely distributed throughout the cytoplasm. The yellow fluorescence in the merged images showed that BDA-ICG and ICG appeared to be distributed in all three organelles. Also, the quantitative analysis results showed that BDA-ICG and ICG in cells exhibited the similar fluorescence distribution to organelle-specific probes. In all groups, the Pearson Correlation Coefficient value was greater than 0.5 and Manders Overlap Coefficient value was greater than 0.6, which demonstrated that BDA-ICG and ICG colocalized with organelles.

During the co-incubation, both BDA-ICG and ICG were able to be absorbed by the neural cells, diffusely distributed throughout the cytoplasm, which supported that they were capable of imaging in neurons and nerve structures in vivo. Also, we noticed that BDA-ICG and ICG might not be organelle-specific, for all the three organelles showed signals of BDA-ICG or ICG, which was consistent with the results

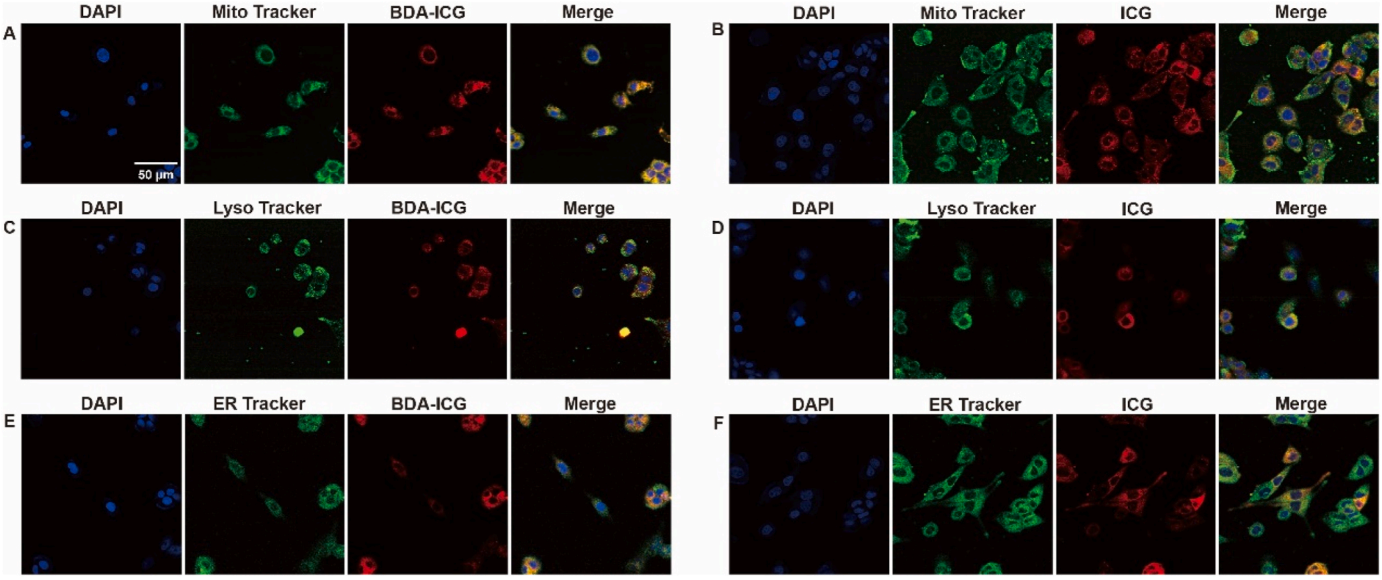

Fig. 3. Intracellular trafficking and distribution of BDA–ICG. BDA-ICG (A, C and E) and ICG (B, D and F) co-localize with organelle-specific fluorescent probes in PC12 cells respectively.

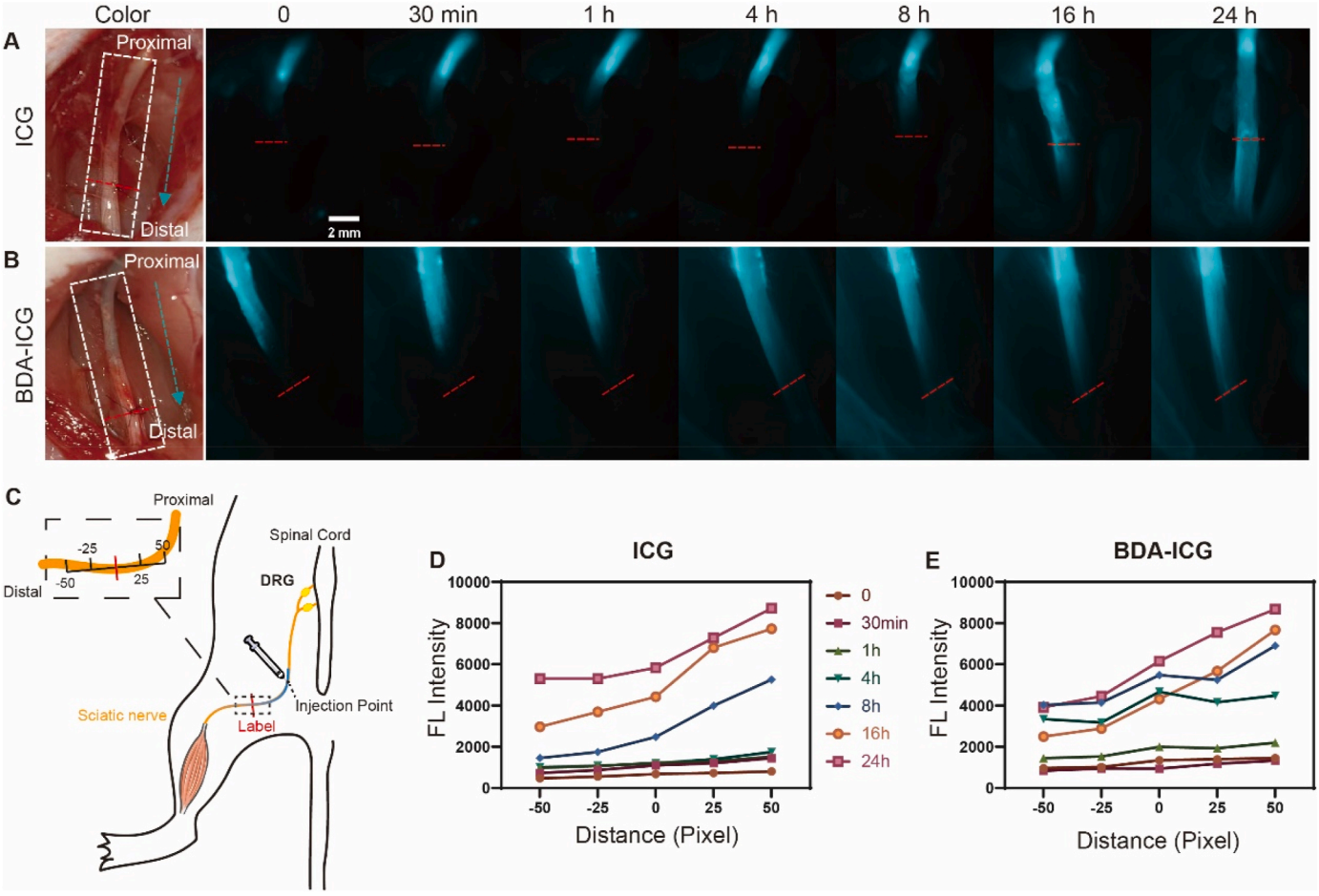

Fig. 4. In vivo monitoring antegrade tracing in peripheral nerve system within 24 h. (A, B) NIR-II imaging of sciatic nerve with ICG and BDA-ICG respectively at different time points (0–24 h post-injection) (Excitation wavelength: 808 nm; Filter: 1000 LP; Exposure time: 100 ms; Laser Power: 102.8 mW cm^{-2}). Red dotted line: the 10-0 nylon label. (C) Schematic overview of sciatic nerve injection for antegrade tracing. (D, E) Changes in PL intensity of the distal and proximal regions around the labeled site during the time course (1 pixel = 0.02 mm).

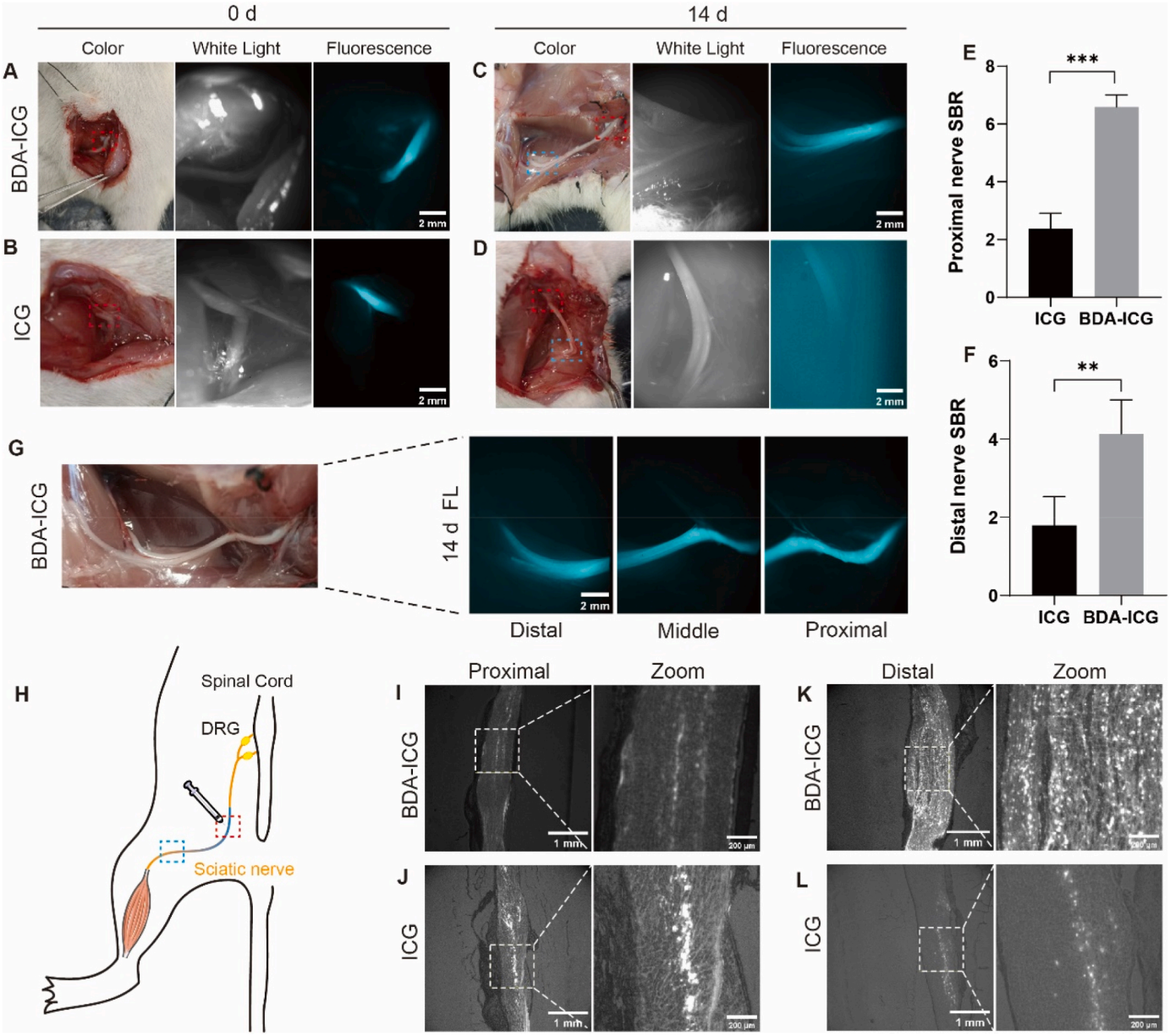

Fig. 5. Long-term in vivo NIR-II fluorescence imaging of the antegrade tracing in peripheral nerve system. (A, B) White light photograph and NIR-II fluorescence images of the injection site (red dotted box) of BDA-ICG and ICG on 0 d and the (C, D) distal part of nerve (blue dotted box) on 14 d post-injection (Excitation wavelength: 808 nm; Filter: 1000 LP; Exposure time: 100 ms; Laser Power: 102.8 mW cm^{-2}). The nerve-background ratio of (E) proximal and (F) distal part of sciatic nerve were recorded. (G) Imaging of the whole nerve from the injection site to the distal with BDA-ICG on 14 d post-injection. (H) Schematic overview of sciatic nerve injection for long-term antegrade tracing. Fluorescence imaging of longitudinal section of sciatic nerve on 14 d post-injection with BDA-ICG (I, K) and ICG (J, L).

reported in previous studies regarding the intracellular distribution of ICG [29,30].

3.4. Anterograde tracing with BDA-ICG and ICG in PNS

To investigate the neural tracing ability of BDA-ICG and ICG in peripheral nerves, we managed to perform intraneural injection of the ICG (5 μL, 0.1 μg/μL) and BDA-ICG (5 μL, 1 μg/μL) in sciatic nerve of rats (Fig. S3). The schematic diagram of the operation process is shown in Fig. 4 C. We labeled the distal part to the injection site with a 10-0 nylon suture as a mark to judge whether BDA-ICG and ICG could be transported from the injection site to the distal part of the nerve. Once the fluorescence signal passed the labeled site, it indicated that the BDA-ICG had been anterogradely transported within the nerve. After the intraneural injection, we tracked and dynamically observed the region of interest for 24 h. During the observation, the fluorescence signals in both BDA-ICG and ICG groups clearly showed a tendency to move from the injection site to the distal labeled site, and the fluorescence signals within the nerves had crossed the labeled site at 24 h post-injection (Fig. 4A and B). In order to more clearly exhibit the process of the anterograde transport of BDA-ICG and ICG, we quantitatively analyzed the change of fluorescence signals in different sites of the nerve with time. Here, the labeled site was defined as the midpoint, and the its distal and proximal part were denoted as negative and positive respectively. According to the direction and distance to the labeled site, we recorded the fluorescence signals of the other four selected sites as shown in Fig. 4C. Taking the labeling site as an example, the fluorescence signal intensity at this point showed a trend of growth within 24 h post-injection (Fig. 4D and E). Though the signal intensity did not change obviously in the initial 1 h, both groups reached maximum signal

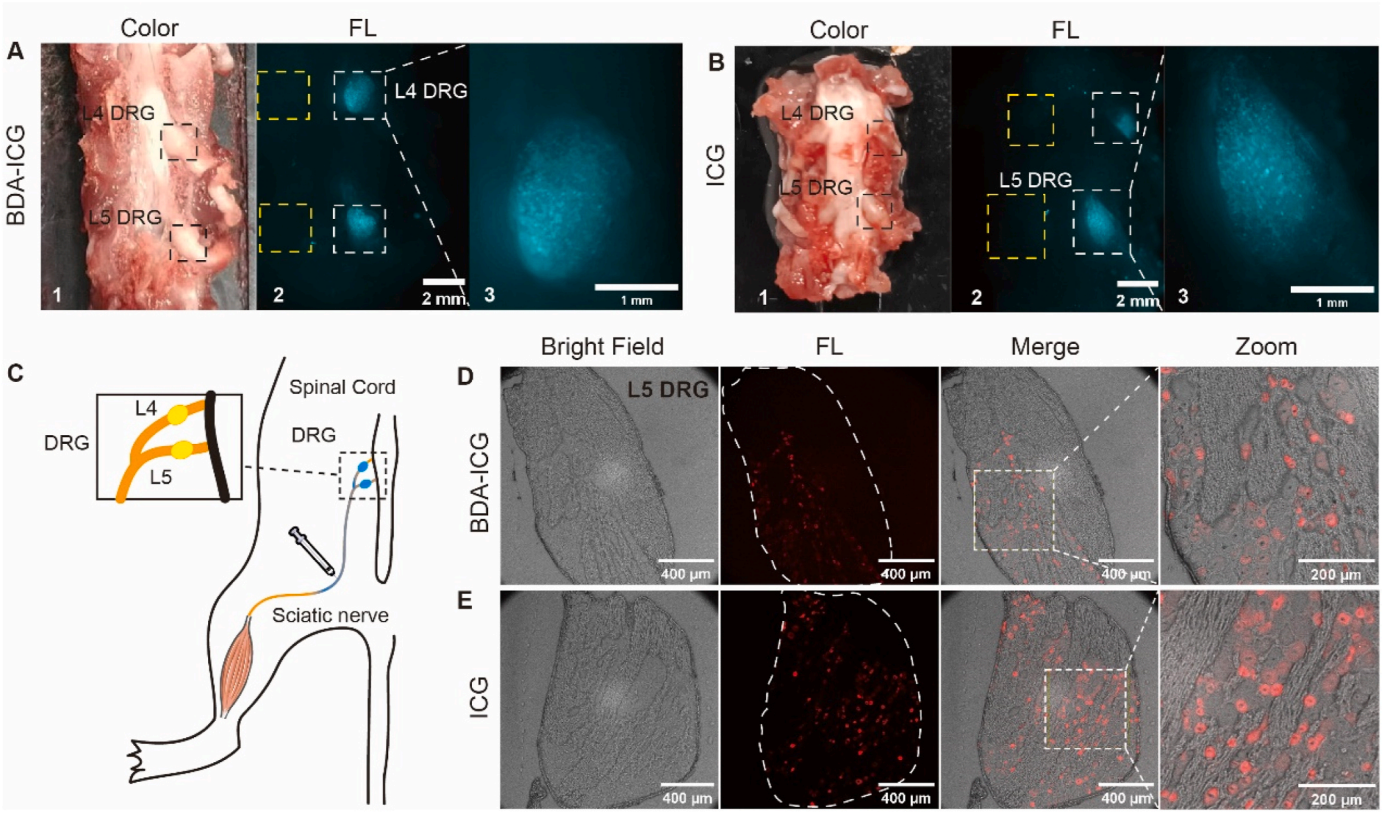

Fig. 6. In vitro NIR-II fluorescence imaging of the retrograde tracing in peripheral nerve system. Ipsilateral and contralateral L4 and L5 DRG showed different fluorescent signals at 24 h after being injected BDA-ICG (A) or ICG (B). (A2 and B2: Yellow dashed box = contralateral DRG. White dashed box = ipsilateral DRG) (Excitation wavelength: 808 nm; Filter: 1000 LP; Exposure time: 100 ms; Laser Power: 102.8 mW cm^{-2}). (C) Schematic overview of sciatic nerve injection to label ipsilateral L4 and L5 DRG. Tissue sections of L5 DRG with BDA-ICG (D) and ICG (E).

intensity at 24 h post-injection. Also, the fluorescence signal intensity at each of the five selected sites exhibited a general trend of gradual decrease from proximal to distal within 24 h following injection, which was consistent with the results of the in vivo imaging. To further understand where the BDA-ICG was distributed, the longitudinal sections and transection sections of the sciatic nerve were triple immunofluorescence stained at 24 h post injection (Fig. S5), and BDA-ICG mainly located in green area (NF200), which was believed to be axons.

These dynamically recorded images confirmed the potential use of BDA-ICG and ICG as anterograde tracers. Both BDA-ICG and ICG were able to be absorbed by the peripheral nerves at the injection site and then transported to the distal part of the nerves. Within the first 1 h post-injection, no significant fluorescent signal movement in nerves was observed. In this case, it is reasonable to assume that the observed results of the anterograde transport of the BDA-ICG and ICG within the nerve is a function of the internal structure of the nerve tissue rather than caused by injected into hollow vascular tissues such as blood vessels or lymph, in which fluorescent signals would appear as soon as the dyes are administrated. The gradual increase in signal intensity at the labeled site within 24 h post-injection, as well as the fact that the proximal signal was higher than that of the distal, all suggest that BDA-ICG and ICG were capable of being transported and moved within the nerves, rather than just being stagnant. Our result is diametrically opposed to the conclusions previously reported by a group who concluded that ICG did not have a good axonal transport capacity due to its high hydrophobicity [31]. We speculated that the observed variability in results could stem from multiple factors, including the experimenter's manipulation, dye concentration and dosage, and observation and analytic techniques. As shown in Fig. 4A and B, ICG seems to have better transport capacity and faster transport speed than BDA-ICG for it crossed the labeled site much more than BDA-ICG group did at 24 h post-injection. However, our replicate experiments showed that the transport effects of these two dyes showed no difference over 24 h and susceptible to the factors mentioned above. Besides, the immunofluorescence staining showed BDA-ICG were mainly located in axons rather than myelin. In conclusion, we successfully observed and confirmed that BDA-ICG and ICG possess the ability of anterograde transport.

Next, we further explored whether ICG and BDA-ICG could persist stably in the peripheral nerves of living animals (Fig. 5H). We performed intraneural injection of ICG and BDA-ICG on 0 d (Fig. 5A and B), then the rats were euthanized and the sciatic nerve was exposed on 14 d post-injection. The sciatic nerve fluorescence signals of the ICG and BDA-ICG groups showed significant differences on 14 d after administration. The in vivo imaging showed that BDA-ICG had better nerve imaging result than the ICG group, with a stronger contrast between the nerve and the surrounding background (Fig. 5C and D). Quantitative analysis of the SBR at the proximal (red dashed box) and distal (blue dashed box) positions of the sciatic nerve on 14 d post-injection showed that the BDA-ICG group had higher nerve-to-background ratio than the ICG group did (Fig. 5E and F). The whole part of sciatic nerve from the injection site to the distal bifurcation in BDA-ICG group was acquired and exposed on the last day and the bifurcation of sciatic nerve were clearly distinguished with NIR-II imaging (Fig. 5 G). The sciatic nerves of both groups were harvested and sectioned along the long axis. Then, the sections were observed under a fluorescence microscope (Ex: 730 nm). The sections showed that BDA-ICG was more retained in the nerve than ICG (Fig. 5 K and L), and both dyes were clearly distributed in a continuous line along the long axis of the nerve (Fig. 5 I and J).

Although previous data showed a high degree of similarity between the BDA-ICG and ICG in terms of optical properties, distribution after intravenous administration, and anterograde-transport imaging over 24 h, they did show marked differences in long-term stability within the

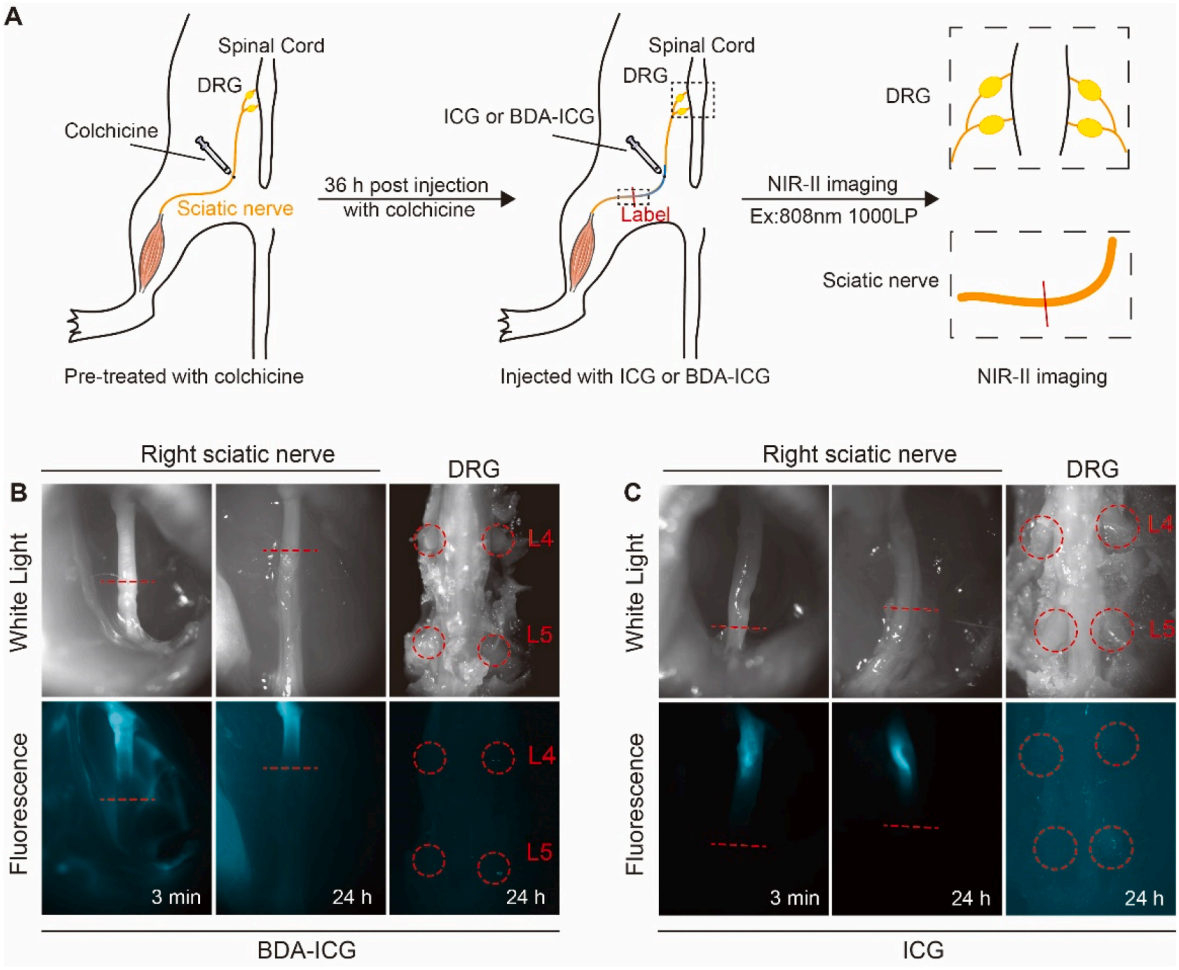

Fig. 7. Anterograde and retrograde tracing with BDA-ICG and ICG in colchicine pre-treated rats. (A) Schematic overview of pre-treating with colchicine. NIR-II imaging of the nerves and DRG in BDA-ICG (B) and ICG (C) group (Excitation wavelength: 808 nm; Filter: 1000 LP; Exposure time: 100 ms; Laser Power: 102.8 mW cm^{-2}).

nerve. BDA-ICG was able to remain stable within the nerve for at least 14 d, however, ICG failed to do so. This discrepancy could be accounted for by the BDA's characteristics. According to previous researches, BDA with a molecular weight of 10 000 MW can persist steadily in the nerve for a maximum of 60 days when utilized for anterograde tracing. This excellent stability in the organism means that BDA-ICG can be used for long-term monitoring and assessment of the anatomical structure and physiological function of nerves. The fluorescence imaging results of the sections also confirmed the better in vivo stability of BDA-ICG compared to ICG, for there were more dyes in the sections of BDA-ICG group. The continuous, linear distribution of the dyes along the long-axis in the nerve sections suggested that the mechanism by which the two dyes can be anterograde transported along the nerves seem to be related to the axoplasmic transport, which was in agreement with our judgment and speculation on their transport mechanisms.

3.5. Retrograde tracing with BDA-ICG and ICG in PNS

The anterograde tracing results indicated that the transport mechanism of BDA-ICG and ICG might be axoplasmic transport, then we wondered whether these two dyes could also be retrogradely transported by axons. The soma of the primary sensory neuron located in the dorsal root ganglion (DRG) and its axons extend to the peripheral. If the dyes can be transported retrogradely within the axon, the dorsal root ganglion corresponding to the nerve injected with the dyes will show fluorescent signals. Based on this, we performed intraneural injection of BDA-ICG or ICG into the sciatic nerve of rats unilaterally (Fig. 6C). At 24 h post-injection, we found that the ipsilateral L4 DRG and L5 DRG both exhibited obvious fluorescent signals and were clearly distinguished from the surrounding tissues (Fig. 6A and B), whereas those on the contralateral side did not exhibit fluorescent signals (Fig.S6 A and B). It was interesting that when we enlarged the magnification of observation with the NIR-II continuous-magnification stereomicroscope, we observed some fluorescent dot-like structures at different spatial locations in the ipsilateral L4 and L5 DRGs, making them honeycomb-like structures (Fig. 6 A3 and B3). In order to learn more about these fluorescent dot-like structures, we harvested the ipsilateral L5 DRG and made frozen sections, which were observed under the fluorescence microscope (Ex:730 nm). Those fluorescent dot-like structures were found out to be primary sensory neurons and BDA-ICG and ICG were specially accumulated in these cells (Fig. 6D and E).

The fluorescent primary sensory neurons in DRGs demonstrated that both BDA-ICG and ICG could be retrogradely transported to the neuron soma and light up the corresponding DRGs within 24 h post-injection. They showed great potential to be used as fast retrograde tracers. However, not all cells or neurons in DRGs showed fluorescence signals. We postulated that not all axons could equally absorb and transport the dyes following intraneural injection, but only a subset of the more vulnerable or injured axons could do so. In addition, the projections of primary sensory neurons in the DRGs are distributed throughout the limb, not just within the sciatic nerve. Maybe that was why only a small fraction of primary sensory neurons were illuminated in the retrograde

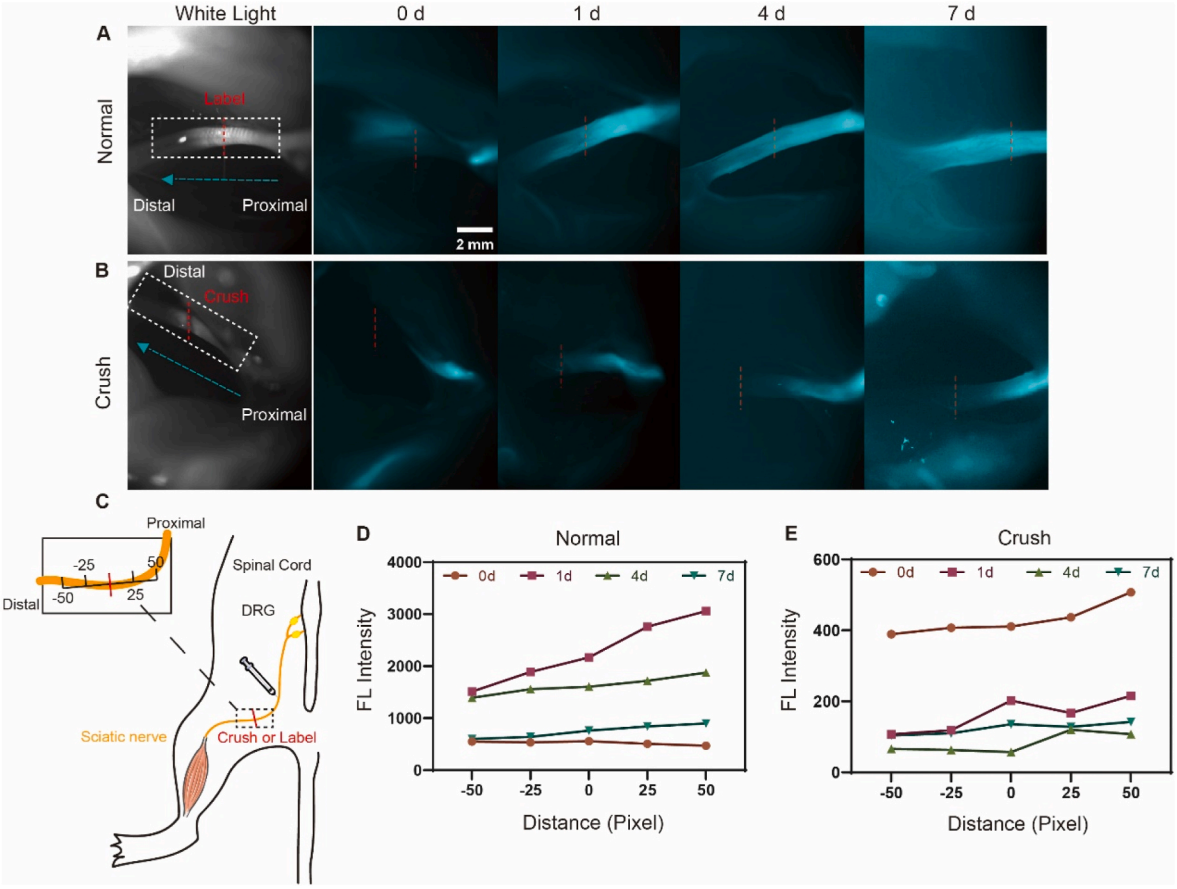

Fig. 8. In vivo NIR-II imaging of BDA-ICG in rat with sciatic nerve injury. (A, B) White light photograph of the region of interest and NIR-II fluorescence images of the normal group compared with the crush group in a time course (0 d, 1 d, 4 d, 7 d post-injection) (Excitation wavelength: 808 nm; Filter: 1000 LP; Exposure time: 100 ms; Laser Power: 102.8 mW cm^{-2}). Red dotted line in crush group indicates injury site. (C) Schematic illustration of in vivo monitoring of BDA-ICG in injured models. (D, E) Changes in PL intensity of the distal and proximal regions of the labeled site during the time course (1 pixel = 0.02 mm).

tracing experiment. The method of intraneural injection drug delivery demonstrated good restriction, as the dye was only delivered into the injected nerves, sparing other nerves from unwanted impacts, which met the requirements for accurate imaging and targeted medication delivery. In conclusion, we demonstrated that BDA-ICG and ICG have the potential for retrograde tracing and that they can be specifically taken up by sensory neurons in the DRGs.

3.6. Colchicine inhibition of axonal transport of BDA-ICG and ICG

Though we have successfully observed the transport of BDA-ICG and ICG in sciatic nerve bi-directionally, the exact transport mechanisms involved have not been directly illuminated yet. Microtubules in axons are the primary routes of transportation for the vast majority of substances within the nerve and they are susceptible to colchicine, which could easily inhibit polymerization of microtubule proteins and thereby block the microtubule-dependent transport [32,33]. To better understand how BDA-ICG and ICG were transported in axons within peripheral nerves, we locally injected colchicine into the sciatic nerves to destroy the microtubules and then injected BDA-ICG and ICG into the colchicine pre-treated sciatic nerves to see whether these dyes could transport along the peripheral nerves (Fig. 7 A). Besides, we performed immunofluorescence staining on nerve sections of no-colchicine group to analyze the distribution of microtubules and BDA-ICG or ICG.

The NIR-II imaging results showed that the fluorescence of both BDA-ICG and ICG just remained at the injection sites and no obvious fluorescence signals appeared in the corresponding DRGs (Fig. 7B and C). The colocalization of β-tubulin and BDA-ICG or ICG in immunofluorescence staining sections of nerves also showed that BDA-ICG and ICG were located mainly in microtubules (Fig. S7). The two dyes could transport within the axons successfully only when the function of microtubules was normal. These findings all demonstrated that the microtubules were the main mechanisms for the transport of BDA-ICG and ICG. To our knowledge, this was the first time that ICG was demonstrated to be transported by microtubules with NIR-II imaging.

3.7. Real-time monitoring the axon transport in crush injury models

One of the most promising clinical applications of neural tracers is that they could be used to detect the functional integrity of substance transport within nerve axons, which is essential for the functional recovery of injured nerve. BDA-ICG and ICG has shown good in vivo properties as NIR-II neural tracers, and we decided to further explore whether these NIR-II neural tracers could be used to identify peripheral nerve injury by in vivo imaging. We constructed a unilateral crush injury model by clamping the sciatic nerve, and the injury site was labeled with 10-0 nylon suture (Fig. 8C). We chose BDA-ICG to perform long-term tracing observation experiments after axonal injury for it has better long-term stability and higher nerve-to-background contrast in vivo than ICG. The control group was a healthy sciatic nerve labeled with 10-0 nylon suture distal to the injection site. After the crush injury model was established, BDA-ICG was injected into the sciatic nerve. In vivo imaging of the labeled site in control group quickly showed obvious signals on 1 d post-injection, and the distal end of the nerve remained high fluorescence signals on 7 d post-injection (Fig. 8 A). However, in the injury group, the fluorescence imaging showed different results.

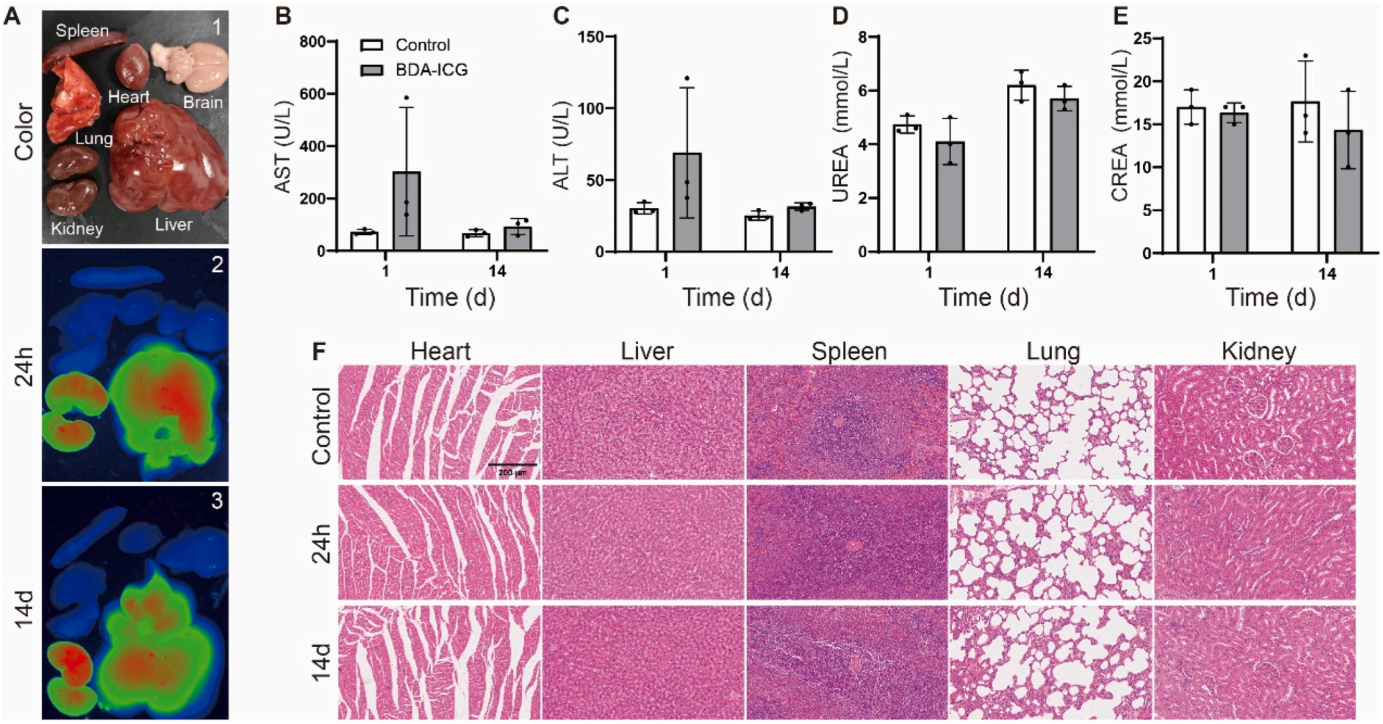

Fig. 9. Biosafety of BDA-ICG. Bright field photograph (A) and NIR-II fluorescence images of the major organs harvested from the rats in the BDA-ICG group at 24 h and on 14 d post-injection (Excitation wavelength: 808 nm; Filter: 1000 LP; Exposure time: 500 ms; Laser Power: 116.9 mW cm^{-2}). Biochemistry results of the control group and the BDA-ICG injected group at 1 d and on 14 d post-injection. Aspartate aminotransferase (B), alanine transaminase (C), urea (D), creatinine (E). (F) Representative H&E stained images of the major organs, including the heart, liver, spleen, lungs and pancreas, collected from the control and BDA-ICG injected rats at 24 h and on 14 d post-injection.

Although the fluorescent signal had already passed through the injury site on day 1 post-injection, the signal around the injury site gradually weakened from 1 d to 7 d post-injection (Fig. 8 B). On 7 d post-injection, the fluorescent signal was obvious only at the proximal part to the injury site, and there was no obvious signal in the injury site. In order to more clearly exhibit the process of the anterograde transport of the dyes in injured nerves, we again quantitatively analyzed the change of fluorescence signals in different sites of the nerve with time. We defined the labeled site as the midpoint, and its distal and proximal part were denoted as negative and positive respectively. According to the direction and distance to the labeled site, we recorded the fluorescence signals of the other four sites as shown in Fig. 8C. The results showed that the labeled site in the normal group soon reached the maximal signal intensity on 1 d post-injection, and then the fluorescence signals gradually decreased in the following days, but neither of them was lower than that on 0 d post-injection (Fig. 8 D). However, in the injury group, the maximum signal intensity of the injury site emerged on 0 d post-injection, then decreased rapidly from 0 d to 1 d post-injection, and never surpassed the maximum signal intensity in the following days (Fig. 8 E).

The trends of fluorescence signal over time of the two groups showed significant differences. This difference could be judged within 1 d after drug administration, which provided the possibility of determining whether the axonal transport function of the damaged nerve was normal or not in an early and timely manner. The results of the injury group confirmed that the dye could no longer be transported through the axon when the normal axonal structure was destroyed. In addition, during the whole observation period, we found the fluorescence signal at the injury site gradually weakened over time. We speculated that this change seemed to be related to the process of Wallerian degeneration following peripheral nerve injury. In this regard, we designed another experiment to exclude the effect of Wallerian degeneration on the dye distribution. We performed intraneural injection of BDA-ICG (same as above) seven days after sciatic nerve crush injury. On 14 d post-injection, we observed that the fluorescent signal was distributed only at the injury site and its proximal but not distal (Fig. S8), which indicated the damaged axonal integrity and poor axonal regeneration. In conclusion, our results suggested that BDA-ICG could help identify the injured nerves within 24 h and track the extent of the wounded nerve's long-term recovery. It has good prospects for early clinical diagnosis of axonal injury and predicting the prognosis of the injured nerve.

3.8. *Biosafety of BDA-ICG after intraneural injection*

Since ICG is an FDA-approved drug, we did not discuss the biosafety of ICG here. We explored the distribution of BDA-ICG within major organs after intraneural injection of BDA-ICG. The major organs of the rats were harvested at 24 h and on 14 d post-injection respectively, and the liver and the kidney showed high fluorescence signals in the both time points (Fig. 9 A). In view of the long-term accumulation of dye in the liver and kidney, we monitored the blood biochemistry changes of the rats throughout the trial. The AST and ALT in the BDA-ICG group showed greater heterogeneity at 24 h post-injection, and were not significantly different from the control group on 14 d post-injection (Fig. 9B and C). The UREA and CREA were just not significantly different from the control group both at 24 h and on 14 d post-injection (Fig. 9D and E). Also, we performed H&E sections of the main internal organs of the experimental group at 24 h and on 14 d post-injection, and no obvious pathological changes were found (Fig. 9 F).

Different routes of administration may correspond to different metabolic pathways. After intraneural injection, BDA-ICG was detected in the liver and kidney for at least 14 d. This was different from the previously described results of visceral distribution at 24 h after intravenous injection, in which the dye was quickly metabolized and only the liver retained the signal after 24 h. We postulated that this difference could be caused by the slow metabolism of lymphatic and trophic

vascular structures in the neural tissues, as well as the slow transport of the dye by axons and neuronal cells to the extracellular compartments. Long-term hepatic and renal physiological function evaluations did not observe significant pathologic damage, and the H&E section results seemed to demonstrate a favorable long-term safety profile for BDA-ICG.

4. Limitation

Though our results demonstrated that ICG and BDA-ICG could both be transported from the terminal to the neuron soma within the axons, there are still some questions need to be better explained by further investigations. First, it seems not all BDA-ICG and ICG molecule could be transported through the axons. There are both some BDA-ICG and ICG sustaining around the injection point in the longitudinal section. One possible reason for this is the so-called stop and go traffic in axons, one of the main hypotheses about the axonal transport, in which the cargo just moves about 2–3 mm per day and to be exclusively anterograde [34]. Also, not all BDA-ICG and ICG could be absorbed by axons, in this way they may react with the structure around the axons, causing them to stay where they are for a long time. Second, the velocity of the transportation of BDA-ICG and ICG in peripheral nerve in vivo has not been well investigated in our research. Usually, the transport speed in axons is recorded and tested in one single axon at a scale bar of 2–5 μm [35], which means it is challenging to figure out the exact speed rate of BDA-ICG and ICG in living animals like rats and often need highly advanced imaging instruments and equipment. Our imaging results could show a rough speed of the neural tracing, however it is quite susceptible to many factors, such as the operator's manipulations and individual differences in rat. These questions need be further explored.

5. Conclusion

This is the first time that the peripheral nerve function is dynamically monitored in vivo by fluorescent neural tracing techniques based on NIR-II fluorescence imaging. ICG shows great potential to be used as a neural tracer with NIR-II imaging characteristics. What's more, a novel tracer BDA-ICG was successfully developed by conjugating BDA with ICG, which was able to be selectively taken up by primary sensory neurons in DRGs and bilaterally transported within axons in the peripheral nervous system of the rat. Our results show that BDA-ICG possesses a longer shelf-life and higher nerve-to-background ration than ICG in peripheral nerve. More importantly, we managed to use BDA-ICG to identify the injured peripheral nerve from the healthy one by in vivo NIR-II fluorescence imaging within just 24 h post the injection, which showed excellent prospects to be applied in fundamental and practical studies.

CRediT authorship contribution statement

Xiaoqi Yang: Writing – review & editing, Writing – original draft, Visualization, Methodology, Investigation, Conceptualization. **Yuanyi Wang:** Investigation, Funding acquisition. **Chunrong Qu:** Visualization, Methodology. **Boyu Tan:** Visualization, Methodology. **Minjin Wang:** Investigation. **Senrui Li:** Visualization. **Jinsheng Huang:** Visualization. **Jiangnan Li:** Visualization. **Mengyuan Fang:** Supervision, Project administration, Funding acquisition. **Zhen Cheng:** Supervision, Project administration. **Nan Zhou:** Writing – review & editing, Writing – original draft, Supervision, Project administration, Funding acquisition, Conceptualization.

Declaration of competing interest

The authors declare that they have no known competing financial interests or personal relationships that could have appeared to influence the work reported in this paper.

Data availability

Data will be made available on request.

Acknowledgements

N.Z. acknowledges the support of National Natural Science Foundation of China (82071388), Excellent Youth Science Foundation of Henan Province (212300410077), Joint Fund for Science and Technology R&D Program of Henan Province (232301420063), Research fund for Overseas Returned Scholars of Human Resources and Social Security in Henan Province (2024-4-4), Excellent Youth Talent Program of Zhengzhou University (2023). M.F. acknowledges the support of Key Research Project of Henan Educational Committee (23A320063), International Cultivation of Henan Advanced Talents (ICHAT) program (2023-25-47), Medical Science and Technology Research Program of Henan Province (SBGJ202303034). Y.W. acknowledges the support of National Natural Science Foundation of China (82372498), Jilin Provincial Department of Science and Technology (20230204049YY), the Excellent Youth Science Foundation of Changchun City (2023), Norman Bethune Program of Jilin University (2022B04).

Appendix A. Supplementary data

Supplementary data to this article can be found online at https://doi.org/10.1016/j.mtbio.2024.101084.

References

[1] X. Navarro, Meritxell Vivó, Antoni Valero-Cabré, Neural plasticity after peripheral nerve injury and regeneration, Prog. Neurobiol. 82 (4) (2007) 163–201.
[2] William W. Campbell, Evaluation and management of peripheral nerve injury, Clin. Neurophysiol. 119 (9) (2008) 1951–1965.
[3] Michael J. Aminoff, Richard B. Weiskopf, Electrophysiologic testing for the diagnosis of peripheral nerve injuries, The Journal of the American Society of Anesthesiologists 100 (5) (2004) 1298–1303.
[4] Stephanie L. Barnes, Thomas A. Miller, Neil G. Simon, Traumatic peripheral nerve injuries: diagnosis and management, Curr. Opin. Neurol. 35 (6) (2022) 718–727.
[5] Rui-Qin Yang, et al., Surgical navigation for malignancies guided by near-infrared-II fluorescence imaging, Small Methods 5 (3) (2021) 2001066.
[6] Songjiao Li, et al., Recent progresses in NIR-I/II fluorescence imaging for surgical navigation, Front. Bioeng. Biotechnol. 9 (2021) 768698.
[7] Wenqian Wang, Jillian Clark, Guangzhao Mao, Neuroanatomical tract tracers: not just for neural tracing anymore, ACS Appl. Bio Mater. 6 (4) (2023) 1380–1397.
[8] Nan Zhou, et al., A novel fluorescent retrograde neural tracer: cholera toxin B conjugated carbon dots, Nanoscale 7.38 (2015) 15635–15642.
[9] Yang Liu, et al., A brand-new generation of fluorescent nano-neural tracers: biotinylated dextran amine conjugated carbonized polymer dots, Biomater. Sci. 7 (4) (2019) 1574–1583.
[10] Yueqi Zhao, et al., Red fluorescent AuNDs with conjugation of cholera toxin subunit B (CTB) for extended-distance retro-nerve transporting and long-time neural tracing, Acta Biomater. 102 (2020) 394–402.
[11] Chunyan Li, et al., Advanced fluorescence imaging technology in the near-infrared-II window for biomedical applications, J. Am. Chem. Soc. 142 (35) (2020) 14789–14804.
[12] Yishen Liu, et al., Versatile types of inorganic/organic NIR-IIa/IIb fluorophores: from strategic design toward molecular imaging and theranostics, Chem. Rev. 122 (1) (2021) 209–268.
[13] Michaela B. Reinhart, et al., Indocyanine green: historical context, current applications, and future considerations, Surg. Innovat. 23 (2) (2016) 166–175.
[14] Shoujun Zhu, et al., Near-infrared-II (NIR-II) bioimaging via off-peak NIR-I fluorescence emission, Theranostics 8 (15) (2018) 4141.
[15] Jarmo T. Alander, et al., A review of indocyanine green fluorescent imaging in surgery, Journal of Biomedical Imaging 2012 (2012), 7-7.
[16] Lei G. Wang, et al., Nerve visualization using phenoxazine-based near-infrared fluorophores to guide prostatectomy, Adv. Mater. (2023) 2304724.
[17] Kunshan He, et al., Near-infrared intraoperative imaging of thoracic sympathetic nerves: from preclinical study to clinical trial, Theranostics 8 (2) (2018) 304.
[18] Kunshan He, et al., Intraoperative near-infrared fluorescence imaging can identify pelvic nerves in patients with cervical cancer in real time during radical hysterectomy, Eur. J. Nucl. Med. Mol. Imag. 49 (8) (2022) 2929–2937.
[19] Elsa Díaz-Montes, Dextran: sources, structures, and properties, Polysaccharides 2 (3) (2021) 554–565.
[20] C.L. Veenman, A. Reiner, M.G. Honig, Biotinylated dextran amine as an anterograde tracer for single-and double-labeling studies, J. Neurosci. Methods 41 (3) (1992) 239–254.

[21] Anton Reiner, et al., Pathway tracing using biotinylated dextran amines, J. Neurosci. Methods 103 (1) (2000) 23–37.
[22] J.L. Lanciego, F.G. Wouterlood, A half century of experimental neuroanatomical tracing, J. Chem. Neuroanat. 42 (3) (2011) 157–183.
[23] Bonghwan Chon, et al., Indocyanine green (ICG) fluorescence is dependent on monomer with planar and twisted structures and inhibited by H-aggregation, Int. J. Mol. Sci. 24 (17) (2023) 13030.
[24] Fellipy S. Rocha, et al., Experimental methods in chemical engineering: ultraviolet visible spectroscopy—UV-Vis, Can. J. Chem. Eng. 96 (12) (2018) 2512–2517.
[25] Lihui Duan, et al., PDGFRβ cells rapidly relay inflammatory signal from the circulatory system to neurons via chemokine CCL2, Neuron 100 (1) (2018) 183–200.
[26] Hongkang Xu, et al., Coumarin-based fluorescent probes for super-resolution and dynamic tracking of lipid droplets, Anal. Chem. 91 (1) (2018) 977–982.
[27] Thais Federici, et al., A means for targeting therapeutics to peripheral nervous system neurons with axonal damage, Neurosurgery 60 (5) (2007) 911–918.
[28] T. Desmettre, J.M. Devoisselle, S. Mordon, Fluorescence properties and metabolic features of indocyanine green (ICG) as related to angiography, Surv. Ophthalmol. 45 (1) (2000) 15–27.
[29] Nobuhiko Onda, et al., Preferential tumor cellular uptake and retention of indocyanine green for in vivo tumor imaging, Int. J. Cancer 139 (3) (2016) 673–682.
[30] Dunwan Zhu, et al., Bubble-generating polymersomes loaded with both indocyanine green and doxorubicin for effective chemotherapy combined with photothermal therapy, Acta Biomater. 75 (2018) 386–397.
[31] Tiffany P. Gustafson, et al., A NIR dye for development of peripheral nerve targeted probes, MedChemComm 3 (6) (2012) 685–690.
[32] B. Fritzsch, Fast axonal diffusion of 3000 molecular weight dextran amines, J. Neurosci. Methods 50 (1) (1993) 95–103.
[33] Nicholas M. Boulis, et al., Intraneural colchicine inhibition of adenoviral and adeno-associated viral vector remote spinal cord gene delivery, Neurosurgery 52 (2) (2003) 381–387.
[34] Anthony Brown, Slow axonal transport: stop and go traffic in the axon, Nat. Rev. Mol. Cell Biol. 1 (2) (2000) 153–156.
[35] Pedro Guedes-Dias, Erika LF. Holzbaur, Axonal transport: driving synaptic function, Science 366 (6462) (2019) eaaw9997.